

# Finite-volume effects in the muon anomalous magnetic moment on the lattice

Christopher Aubin,<sup>a</sup> Thomas Blum,<sup>b</sup> Peter Chau,<sup>c</sup> Maarten Golterman,<sup>c</sup> Santiago Peris,<sup>d</sup>  
Cheng Tu<sup>b</sup>

<sup>a</sup>*Department of Physics & Engineering Physics  
Fordham University, Bronx, New York, NY 10458, USA*

<sup>b</sup>*Physics Department  
University of Connecticut, Storrs, CT 06269, USA*

<sup>c</sup>*Department of Physics and Astronomy, San Francisco State University  
San Francisco, CA 94132, USA*

<sup>d</sup>*Department of Physics and IFAE-BIST, Universitat Autònoma de Barcelona  
E-08193 Bellaterra, Barcelona, Spain*

## ABSTRACT

We investigate finite-volume effects in the hadronic vacuum polarization, with an eye toward the corresponding systematic error in the muon anomalous magnetic moment. We consider both recent lattice data as well as lowest-order, finite-volume chiral perturbation theory, in order to get a quantitative understanding. Even though leading-order chiral perturbation theory does not provide a good description of the hadronic vacuum polarization, it turns out that it gives a good representation of finite-volume effects. We find that finite-volume effects cannot be ignored when the aim is a few percent level accuracy for the leading-order hadronic contribution to the muon anomalous magnetic moment, even when using ensembles with  $m_\pi L \gtrsim 4$  and  $m_\pi \sim 200$  MeV.

## I. INTRODUCTION

A convenient representation for the lowest-order hadronic contribution to the anomalous magnetic moment  $a_\mu = (g - 2)/2$  in terms of an integral over euclidean momentum is given by [1, 2]

$$a_\mu^{\text{LO,HVP}} = \lim_{q_{\text{max}}^2 \rightarrow \infty} a_\mu^{\text{LO,HVP}}[q_{\text{max}}^2] , \quad (1.1)$$

$$a_\mu^{\text{LO,HVP}}[q_{\text{max}}^2] = 4\alpha^2 \int_0^{q_{\text{max}}^2} dq^2 f(q^2) \hat{\Pi}(q^2) ,$$

where  $m_\mu$  is the muon mass,

$$f(q^2) = m_\mu^2 q^2 Z^3(q^2) \frac{1 - q^2 Z(q^2)}{1 + m_\mu^2 q^2 Z^2(q^2)} ,$$

$$Z(q^2) = \left( \sqrt{(q^2)^2 + 4m_\mu^2 q^2} - q^2 \right) / (2m_\mu^2 q^2) , \quad (1.2)$$

and  $\hat{\Pi}(q^2) \equiv \Pi(q^2) - \Pi(0)$  is the subtracted hadronic vacuum polarization. The vacuum polarization  $\Pi(q^2)$  is defined from the hadronic electromagnetic current two-point function,  $\Pi_{\mu\nu}(q)$ , via

$$\Pi_{\mu\nu}(q) \equiv \int d^4x e^{iqx} \langle J_\mu(x) J_\nu(0) \rangle = (q^2 \delta_{\mu\nu} - q_\mu q_\nu) \Pi(q^2) , \quad (1.3)$$

with  $J_\mu(x)$  the hadronic electromagnetic current. The form on the right-hand side of Eq. (1.3) follows from current conservation and rotational symmetry.

While, in principle, a lattice computation of the hadronic vacuum polarization<sup>1</sup> is straightforward, it turns out that a very high accuracy is needed in the region around  $q^2 \sim m_\mu^2/4$ . The reason is that the integrand of Eq. (1.1) is strongly peaked in that region, as illustrated in Fig. 1. In effect, the weight function  $f(q^2)$  acts as a “magnifying glass” of the low-momentum region, where it is hard to obtain lattice data points with small errors. We note that the data points shown in Fig. 1 have been obtained with all-mode averaging (AMA) [3], and thus have errors much reduced in comparison with the state of the art of only a few years ago.<sup>2</sup>

Figure 1 also suggests that finite-volume effects may cause a significant systematic error, because it is the finite-volume quantization of momenta that makes the number of data points in the low- $q^2$  region so sparse. It is our aim in this article to investigate this quantitatively. A more phenomenological study of finite-volume effects appeared in Ref. [5], and a preliminary account of the present work appeared in Ref. [6].<sup>3</sup>

We will restrict ourselves to a rectangular volume  $L^3 \times T$  with periodic boundary conditions in all directions, and we will be interested in the case that  $T > L$ , as is the case for all lattice computations of the hadronic vacuum polarization. While twisted boundary conditions have been considered [7, 8], a generic twist vector reduces the symmetry group of

<sup>1</sup> Or, at least, its connected part.

<sup>2</sup> See, for example, Fig. 1 of Ref. [4].

<sup>3</sup> The results reported in Ref. [6] were based on an incorrect version of Eq. (2.12), and did not take into account taste splittings.

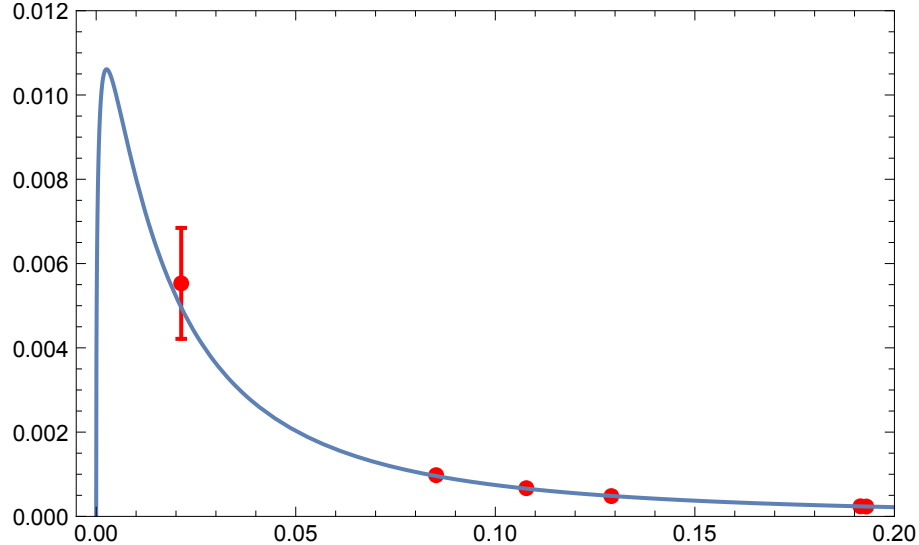


FIG. 1: *Integrand of Eq. (1.1), in arbitrary units ( $q^2$  in  $\text{GeV}^2$ ). The red points represent lattice data from the MILC asqtad ensemble considered in this article, while the blue curve is the product of the weight  $f(q^2)$  and a typical smooth fit to the subtracted vacuum polarization  $\hat{\Pi}(q^2)$ .*

the problem. Thus, the continuum representation of the rotation group according to which  $\Pi_{\mu\nu}(q)$  transforms would reduce to even more representations of the even smaller discrete subgroup, but it would not reduce the size of finite-volume effects given certain values of  $m_\pi L$  and  $m_\pi$ .

This article is organized as follows. In Sec. II we discuss general theoretical considerations based on the Ward–Takahashi identity (WTI) and the irreducible representations of the cubic group, followed by a calculation of the vacuum polarization in finite volume in lowest-order (staggered) chiral perturbation theory (ChPT). In Sec. III, we then compare lattice data for the vacuum polarization with ChPT, and quantify the size of the systematic error due to finite-volume effects on  $a_\mu^{\text{LO,HVP}}$ . We conclude in Sec. IV, and an appendix contains details of the calculation of the finite-volume vacuum polarization in ChPT (generalizing it to the case with twisted boundary conditions).

## II. THEORETICAL CONSIDERATIONS

In an infinite volume and in the continuum limit, symmetry and current conservation implies that the vacuum polarization takes the form (1.3). Current conservation carries over to the lattice, but now a more general decomposition of the vacuum polarization is possible, because the symmetry is reduced. The WTI restricts  $\Pi_{\mu\nu}(q)$  to obey ( $a$  is the lattice spacing)

$$\sum_{\mu} \hat{q}_{\mu} \Pi_{\mu\nu}(q) = 0 , \quad (2.1)$$

$$\hat{q}_{\mu} \equiv \frac{2}{a} \sin(aq_{\mu}/2) . \quad (2.2)$$

Requiring  $\Pi_{\mu\nu}(q)$  to be symmetric in the indices  $\mu$  and  $\nu$ ,<sup>4</sup> and assuming an infinite, isotropic hypercubic lattice, the WTI implies the most general form<sup>5</sup>

$$\begin{aligned} \Pi_{\mu\nu}(q) = & (\delta_{\mu\nu}\hat{q}^2 - \hat{q}_\mu\hat{q}_\nu) \Pi(q) \\ & + \left( \delta_{\mu\nu} \left( \sum_\rho \hat{q}_\rho^4 + \hat{q}_\mu^2\hat{q}_\nu^2 \right) - \hat{q}_\mu^3\hat{q}_\nu - \hat{q}_\mu\hat{q}_\nu^3 \right) \Pi'(q) + \dots, \end{aligned} \quad (2.3)$$

where  $\hat{q}^2 = \sum_\mu \hat{q}_\mu^2$ . While  $\Pi(q)$  is dimensionless,  $\Pi'(q)$  has mass dimension -2. That means that it has to vanish at least quadratically with the lattice spacing  $a$ ; for  $a \rightarrow 0$ , the expression in Eq. (2.3) has to reduce to Eq. (1.3). Here, we will be only interested in the vacuum polarization for very small momenta, and we will thus assume that we can ignore the scaling violations on the second line of Eq. (2.3).

When we restrict ourselves also to a finite volume in the form of a hypercubic box of dimensions  $L^3 \times T$  with periodic boundary conditions, Eq. (2.3) is not the most general form of  $\Pi_{\mu\nu}(q)$  if the hypercubic symmetry is further broken by choosing  $L \neq T$ , as we will discuss next.

### A. Group theory

When we go to a finite periodic volume  $L^3 \times T$  with  $L \neq T$ ,<sup>6</sup> two things happen. First, momenta are quantized,

$$q_i = \frac{2\pi n_i}{L}, \quad i = 1, 2, 3, \quad q_4 = \frac{2\pi n_4}{T}, \quad (2.4)$$

where the  $n_\mu$  are integers. The WTI (2.1) does not restrict the vacuum polarization at zero momentum, and in general, in a finite volume,  $\Pi_{\mu\nu}(0) \neq 0$ .<sup>7</sup> Rather, rotational symmetry implies that it takes the form

$$\Pi_{\mu\nu}(0) = \delta_{\mu\nu} (\Pi_s(0) + \delta_{\mu 4} (\Pi_4(0) - \Pi_s(0))) , \quad (2.5)$$

with  $\Pi_s(0)$  and  $\Pi_4(0)$  constants.<sup>8</sup> For  $T \gg L$  one expects that  $\Pi_4(0) \ll \Pi_s(0)$ . It thus makes sense to consider a subtracted vacuum polarization

$$\begin{aligned} \bar{\Pi}_{\mu\nu}(q) &= \sum_{\kappa\lambda} P_{\mu\kappa}^T (\Pi_{\kappa\lambda}(q) - \Pi_{\kappa\lambda}(0)) P_{\lambda\nu}^T \\ &= \Pi_{\mu\nu}(q) - P_{\mu\nu}^T \Pi_s(0) - P_{\mu 4}^T P_{4\nu}^T (\Pi_4(0) - \Pi_s(0)) , \\ P_{\mu\nu}^T(q) &= \delta_{\mu\nu} - \frac{q_\mu q_\nu}{q^2} , \end{aligned} \quad (2.6)$$

where  $P^T$  is the transverse projector. We projected the subtracted vacuum polarization so that it still satisfies the WTI after the subtraction of its value at zero momentum. Of course, without the subtraction, this projection has no effect, since  $\sum_\mu q_\mu \Pi_{\mu\nu}(q) = \sum_\nu \Pi_{\mu\nu}(q) q_\nu = 0$ .

<sup>4</sup> We will always use only the Noether current in Eq. (1.3).

<sup>5</sup> See also Ref. [9].

<sup>6</sup> We will always consider the case that  $T > L$ .

<sup>7</sup> This, and some of the other observations that follow below, have also been noted in Ref. [10].

<sup>8</sup> For an estimate using ChPT, see the appendix.

Second, the rotation group is reduced to the group of cubic rotations, defined by the irreducible representation (irrep) of 90-degree rotations on the spatial components of momentum. While the infinite-volume form (1.3) contains only one scalar function, this is no longer the case in our finite volume. The tensor  $\bar{\Pi}_{\mu\nu}$  contains five different irreducible sub-structures:

$$\begin{aligned} A_1: \quad & \sum_i \bar{\Pi}_{ii} = (3q^2 - \vec{q}^2) \bar{\Pi}_{A_1} , \\ A_1^{44}: \quad & \bar{\Pi}_{44} = (\vec{q}^2) \bar{\Pi}_{A_1^{44}} , \\ T_1: \quad & \bar{\Pi}_{4i} = -(q_4 q_i) \bar{\Pi}_{T_1} , \\ T_2: \quad & \bar{\Pi}_{ij} = -(q_i q_j) \bar{\Pi}_{T_2} , \quad i \neq j , \\ E: \quad & \bar{\Pi}_{ii} - \sum_i \bar{\Pi}_{ii}/3 = (-q_i^2 + \vec{q}^2/3) \bar{\Pi}_E , \end{aligned} \tag{2.7}$$

where  $\vec{q}^2 = \sum_i q_i^2$ . Equation (2.7) defines five different scalar functions  $\bar{\Pi}_r$ ,  $r \in \{A_1, A_1^{44}, T_1, T_2, E\}$ , which are unrelated by symmetry, since the sub-structures shown here do not transform into each other under cubic rotations. For the spatial diagonal elements, Eq. (2.7) implies that

$$\bar{\Pi}_{ii} = (-q_i^2 + \vec{q}^2/3) \bar{\Pi}_E + (q^2 - \vec{q}^2/3) \bar{\Pi}_{A_1} . \tag{2.8}$$

The irrep  $A_1$  occurs twice in Eq. (2.7), and we distinguish the two with the notation  $A_1$  and  $A_1^{44}$ . Unbarred scalar functions,  $\Pi_r$ ,  $r \in \{A_1, A_1^{44}, T_1, T_2, E\}$ , are defined analogously by replacing components of  $\bar{\Pi}_{\mu\nu}$  by  $\Pi_{\mu\nu}$  on the left-hand side of Eq. (2.7). The WTI implies some relations between these functions. In particular,  $\sum_\mu q_\mu \bar{\Pi}_{\mu 4} = 0$  implies that

$$q_4 \vec{q}^2 (\bar{\Pi}_{T_1} - \bar{\Pi}_{A_1^{44}}) = 0 , \tag{2.9}$$

while  $\sum_\mu q_\mu \bar{\Pi}_{\mu i} = 0$  implies (choosing  $i$  such that  $q_i \neq 0$ )

$$\vec{q}^2 (-\bar{\Pi}_{T_2} + \frac{1}{3} \bar{\Pi}_E + \frac{2}{3} \bar{\Pi}_{A_1}) + q_i^2 (\bar{\Pi}_{T_2} - \bar{\Pi}_E) + q_4^2 (\bar{\Pi}_{A_1} - \bar{\Pi}_{T_1}) = 0 . \tag{2.10}$$

The unbarred  $\Pi_r$  satisfy the same relations.

We note that these scalar functions can still be functions of all cubic invariants that can be made out of  $q_\mu$ . Invariants with dimension larger than 2, like  $\sum_i q_i^4$  have coefficients that are positive power of the lattice spacing, so we will assume that these are negligibly small at the values of  $q_\mu$  we are interested in. That still leaves us with the invariants  $\vec{q}^2$  and  $q_4^2$ .<sup>9</sup> Empirically, we find, however, that the functions  $\bar{\Pi}_r$  are a function of  $q^2$  (or  $\hat{q}^2$ , see below) to a high degree of accuracy.

The unbarred  $\Pi_r$ ,  $r \in \{A_1, A_1^{44}, T_1, T_2, E\}$ , are more singular than the barred  $\bar{\Pi}_r$ . Using Eqs. (2.6) and (2.7), we find that

$$\begin{aligned} \Pi_{A_1} &= \bar{\Pi}_{A_1} + \frac{1}{q^2} \left( \Pi_s(0) + \frac{q_4^2 \vec{q}^2}{q^2(3q^2 - \vec{q}^2)} (\Pi_4(0) - \Pi_s(0)) \right) , \quad q^2 \neq 0 , \\ \Pi_{A_1^{44}} &= \bar{\Pi}_{A_1^{44}} + \frac{1}{q^2} \left( \Pi_s(0) + \frac{\vec{q}^2}{q^2} (\Pi_4(0) - \Pi_s(0)) \right) , \quad \vec{q}^2 \neq 0 , \\ \Pi_{T_1} &= \bar{\Pi}_{T_1} + \frac{1}{q^2} \left( \Pi_s(0) + \frac{\vec{q}^2}{q^2} (\Pi_4(0) - \Pi_s(0)) \right) , \quad q_4 q_i \neq 0 \text{ for some } i , \end{aligned} \tag{2.11}$$

<sup>9</sup> Odd powers of  $q_4$  are excluded because of axis inversion symmetry.

$$\begin{aligned}\Pi_{T_2} &= \bar{\Pi}_{T_2} + \frac{1}{q^2} \left( \Pi_s(0) - \frac{q_4^2}{q^2} (\Pi_4(0) - \Pi_s(0)) \right), \quad q_i q_j \neq 0 \text{ for some } i, j, \\ \Pi_E &= \bar{\Pi}_E + \frac{1}{q^2} \left( \Pi_s(0) - \frac{q_4^2}{q^2} (\Pi_4(0) - \Pi_s(0)) \right), \quad \vec{q}^2 \neq 0 \text{ and } \vec{q}^2 \neq 3q_i^2.\end{aligned}$$

The conditions listed for each case follow from the definitions in Eq. (2.7). Since both  $\bar{\Pi}_r$  and  $\Pi_r$  satisfy the WTIs (2.9) and (2.10), the terms in parentheses in Eq. (2.11) should satisfy these equations, and indeed they do.

One may also define scalar functions  $\hat{\Pi}_r$  as in Eq. (2.7) from the subtracted vacuum polarization but without the projectors present in Eq. (2.6). In that case, the subtracted vacuum polarization does not satisfy the WTI, but this is purely a finite-volume effect. We have that  $\hat{\Pi}_r = \Pi_r$  for  $r \in \{T_1, T_2, E\}$ , and also that  $\hat{\Pi}_{A_1^{44}} = \Pi_{A_1^{44}}$  if  $\Pi_4(0) = 0$ . The latter condition is approximately satisfied for the lattice ensembles we will consider in the sense that  $\Pi_4(0) \ll \Pi_s(0)$ , as a consequence of the fact that  $T \gg L$ . In ChPT we find that  $\bar{\Pi}_{A_1}$  is a smoother function than  $\hat{\Pi}_{A_1}$ , while for the other representations we find that  $\hat{\Pi}_r = \Pi_r$  is smoother than  $\bar{\Pi}_r$ . In Sec. III, we will thus choose to consider the lattice data for  $\bar{\Pi}_{A_1}$  and  $\Pi_r$  for  $r \in \{A_1^{44}, T_1, T_2, E\}$ , even though the difference between  $\hat{\Pi}_r$  and  $\bar{\Pi}_r$  is not visible in the lattice data because of the statistical errors.

Of course, the data we will consider live not only in a finite volume, but also on a lattice. However, since we are interested in the low- $q$  behavior of the vacuum polarization, we will assume that higher-order terms in the lattice spacing (*cf.* the second line of Eq. (2.3)) can be neglected, as mentioned before. The only scaling violations we will take into account are those represented by replacing  $q_\mu$  by  $\hat{q}_\mu$ , defined in Eq. (2.2), and the taste splitting of the Nambu–Goldstone boson (NGB) masses present in the spectrum of lattice QCD with staggered fermions at non-zero lattice spacing. We note that the numerical difference between  $q_\mu$  and  $\hat{q}_\mu$  is tiny, for momenta up to 1 GeV, for the lattice ensemble we will consider in this article.

## B. Chiral perturbation theory

The heuristic picture is that finite volume effects are caused by hadrons traveling “around the world” (*i.e.*, seeing the periodic boundary conditions). The euclidean propagator for a particle with mass  $m$  traveling a distance  $L$  falls like  $e^{-mL}$ . Therefore, finite-volume effects are predominantly felt by the pions, because they are the lightest hadrons present in the theory, and it is thus useful to consider finite-volume effects in ChPT, the effective field theory for pions.<sup>10</sup>

It is well-known that leading-order ChPT does not describe the hadronic vacuum polarization very well already at very low  $q^2$  and pion masses [12].<sup>11</sup> The intuitive reason is that resonance contributions, like that from the  $\rho$ , are important, but only higher orders in ChPT “know” about such resonances (through low-energy constants at higher order). However, by the same argument, ChPT should do much better describing *differences* caused only by finite-volume effects, because those should be dominated by pions, and quite suppressed for

<sup>10</sup> See Ref. [11] for an introduction to applications of ChPT to lattice QCD, including ChPT in a finite volume, partial quenching, and staggered ChPT, as well as references.

<sup>11</sup> For a discussion of  $\Pi_{V-A}$ , see Ref. [13].

all other hadrons. Here we will assume that it is reasonable to study finite-volume effects using leading-order ChPT for pions only. We will then compare the predictions from ChPT with lattice data, to see how this assumption fares, in Sec. III.

The lattice data we will consider have been generated on ensembles with three flavors of sea quarks, up, down and strange. Therefore, at lowest order in ChPT,  $\Pi_{\mu\nu}(q)$  receives loop contributions from all NGBs for a three-flavor theory. However, since the kaon mass is always much larger than the pion mass, we will calculate only the pion loops in ChPT, and compare the result with the lattice data. Any discrepancies may be due to kaon loops, higher orders, *etc.*

The appendix provides some details about the ChPT calculation, and generalizes it to the case of twisted boundary conditions. For periodic boundary conditions the leading-order contribution from pions to the connected part of the vacuum polarization is

$$\begin{aligned} \Pi_{\mu\nu}(q) = \frac{10}{9} e^2 \frac{1}{L^3 T} \sum_p \left[ \frac{4 \sin(p+q/2)_\mu \sin(p+q/2)_\nu}{(2 \sum_\kappa (1 - \cos p_\kappa) + m_\pi^2) (2 \sum_\kappa (1 - \cos(p+q)_\kappa) + m_\pi^2)} \right. \\ \left. - \delta_{\mu\nu} \left( \frac{2 \cos p_\mu}{(2 \sum_\kappa (1 - \cos p_\kappa) + m_\pi^2)} \right) \right], \end{aligned} \quad (2.12)$$

where  $e$  is the electron charge and  $m_\pi$  is the pion mass. We have used a lattice regulator in order to define this expression, and all dimensionful physical quantities in Eq. (2.12) are expressed in units of the lattice spacing. It is straightforward to verify that  $\Pi_{\mu\nu}(0) = 0$  when the momentum sum in Eq. (2.12) is replaced by a momentum integral, by partial integration on the first term in the integral. In the appendix we show that in finite volume  $\Pi_{\mu\nu}(0) \neq 0$ , as a simple application of the Poisson resummation formula, *cf.* Eq. (A16).

Since in the next section we will be comparing ChPT with lattice data obtained with “rooted” staggered fermions, we should amend Eq. (2.12) to what we would have obtained using rooted staggered ChPT [14, 15]. Staggered fermions lead to “taste symmetry breaking,” splitting the degenerate pion spectrum due to lattice artifacts, and this turns out to be a significant effect even at low energy, and therefore we will take this effect into account when comparing with lattice data.<sup>12</sup> We will also use the momenta  $\hat{q}$  introduced in Eq. (2.2) instead of  $q$ , but this amounts to a difference of less than 0.1% even at  $q^2 = 1 \text{ GeV}^2$  for the data we consider in Sec. III.

It is very simple to adapt our result (2.12) (or Eq. (A11) in the appendix) to the staggered case. To lowest order in rooted staggered ChPT, all we need to do is to replace the summand in Eq. (2.12) (or Eq. (A11)) by a weighted average over the taste-split pion spectrum with masses  $m_\pi = m_P, m_A, m_T, m_V$  and  $m_I$ , with, respectively, weights  $1/16, 1/4, 3/8, 1/4$ , and  $1/16$ . We will refer to this version of our result as (lowest-order) SChPT.

### III. LATTICE DATA

In this section, we will consider lattice data for the connected part of the light-quark hadronic vacuum polarization for the asqtad ensemble generated by the MILC collaboration [17] with  $1/a = 3.35 \text{ GeV}$ ,  $m_\pi = 220 \text{ MeV}$ ,  $L/a = 64$  and  $T/a = 144$ .

<sup>12</sup> For an introduction to rooted staggered fermions, and further references, see Ref. [16].

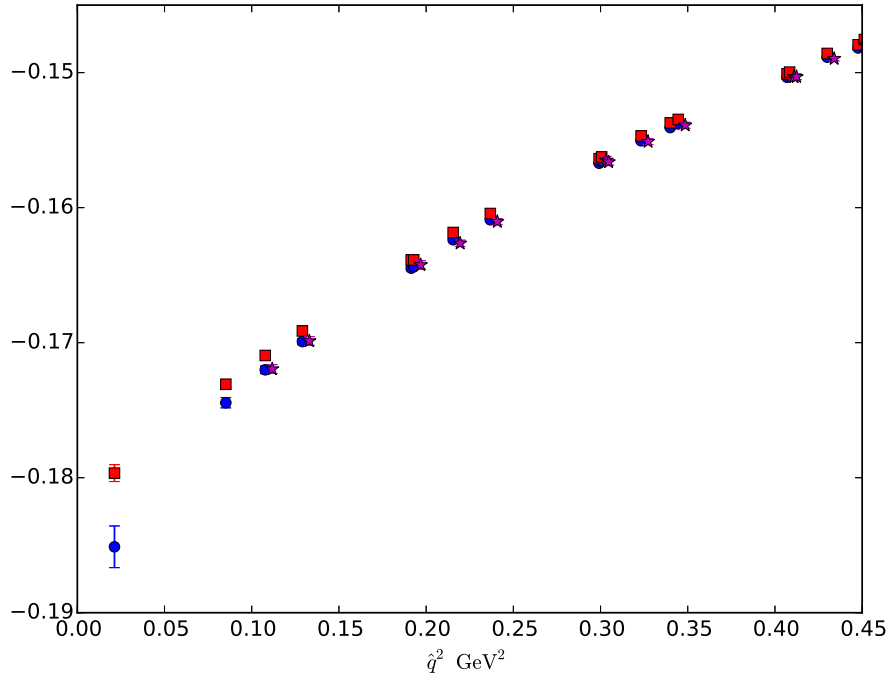


FIG. 2: Low- $\hat{q}^2$  lattice data for the connected part of  $\bar{\Pi}_{A_1}(\hat{q}^2)$  (red squares),  $\Pi_{A_1}(\hat{q}^2)$  (blue circles), and  $\Pi_{A_1^{44}}(\hat{q}^2)$  (purple stars). MILC asqtad ensemble; the purple stars have been horizontally offset by +0.004 GeV<sup>2</sup> for visibility.

For illustration, we show the vacuum polarization for the asqtad ensemble in Fig. 2, with errors obtained using all-mode averaging (AMA) [3]. The red squares show  $\bar{\Pi}_{A_1}(\hat{q}^2)$ , obtained from  $\bar{\Pi}_{\mu\nu}(\hat{q})$  using Eq. (2.7), the blue circles show  $\Pi_{A_1}(\hat{q}^2)$ , and the magenta stars show  $\Pi_{A_1^{44}}(\hat{q}^2)$ , obtained similarly from  $\Pi_{\mu\nu}(\hat{q})$  (they are slightly offset horizontally to make them visible).<sup>13</sup> The difference between these three cases is a finite-volume effect, and clearly visible, thanks to the very small statistical errors obtained with the AMA method. The lattice data for  $\bar{\Pi}_{A_1^{44}}(\hat{q}^2)$  agree, within errors, with those for  $\Pi_{A_1^{44}}(\hat{q}^2)$ .

We will first compare the lattice data to ChPT, in Sec. III A. Since, as explained in Sec. II B, we expect that only finite-volume differences can be sensibly compared, we will limit ourselves to such differences. Then, in Sec. III B, we will use the lattice data to determine  $a_\mu[\hat{q}_{max}^2 = 0.1 \text{ GeV}^2]$  from different irreps, in order to see how finite-volume effects in the data propagate to the anomalous magnetic moment.

### A. Comparison with ChPT

Figure 3 shows a plot similar to Fig. 2, but with the data points computed in lowest-order SChPT. In addition, in ChPT we have access to the values of the vacuum polarization in

<sup>13</sup> The magenta points start at a higher value of  $\hat{q}^2$ , because  $\Pi_{A_1^{44}}(\hat{q}^2)$  vanishes when all spatial components of the momentum vanish, *cf.* Eq. (2.7). In contrast,  $\bar{\Pi}_{A_1}(\hat{q}^2)$  and  $\Pi_{A_1}(\hat{q}^2)$  do not vanish for any non-zero value of the momentum.



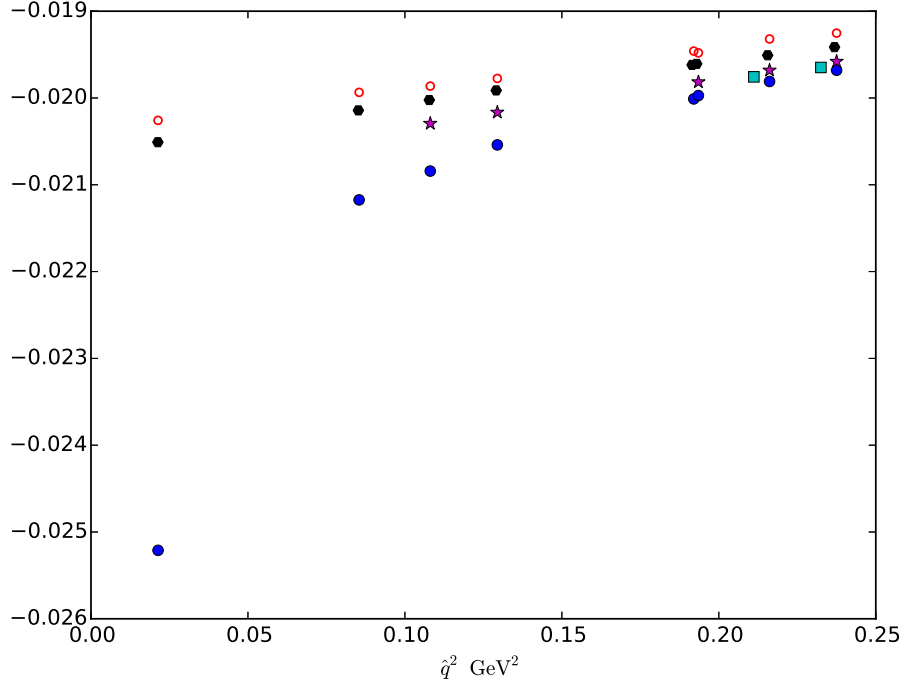


FIG. 3: *Low- $\hat{q}^2$  SChPT points for the connected part of  $\bar{\Pi}_{A_1}(\hat{q}^2)$  (red open circles),  $\Pi_{A_1}(\hat{q}^2)$  (blue filled circles),  $\Pi_{A_1^{44}}(\hat{q}^2)$  (purple stars),  $\Pi_{T_2}(\hat{q}^2)$  (cyan squares), and  $\Pi_{A_1}(\hat{q}^2)$  in infinite volume (black hexagons).*

infinite volume, and infinite-volume points for the same  $\hat{q}^2$  values are shown in black in Fig. 3.<sup>14</sup>

Consistent with what we observe in the lattice data, there is no significant difference between  $\bar{\Pi}_r(\hat{q}^2)$  and  $\Pi_r(\hat{q}^2)$  for all representations except  $r = A_1$ . This is why we omitted  $\bar{\Pi}_{A_1^{44}}(\hat{q}^2)$  and the representations  $T_1$  and  $E$  in Fig. 3. We do show  $\Pi_{T_2}(\hat{q}^2)$  as the two cyan squares all the way to the right.<sup>15</sup> To extract  $\Pi_{T_2}(\hat{q}^2)$  from  $\Pi_{ij}(\hat{q})$  we need two different spatial components of the momentum to not vanish, implying that  $\hat{q}^2 \geq 8\pi^2/L^2 = 0.216 \text{ GeV}^2$  for these points. The  $A_1$  representation is the most interesting case, because it reaches lower momenta than any of the others. It is the only one that does not vanish when only  $\hat{q}_4 \neq 0$ , and the two smallest values of  $\hat{q}^2$  have only  $\hat{q}_4 \neq 0$ ; it is thus the most useful representation to explore the low-momentum behavior of  $\Pi(q^2)$ .

There are clear differences between Figs. 2 and 3. First, the vertical offset is very different. This is not a physical effect, because the quantities plotted are logarithmically divergent in

<sup>14</sup> In reality, the black points are  $\Pi_{A_1}(\hat{q}^2)$  for  $L/a = 128$ ,  $T/a = 288$ . On the scale of the plot, the differences between infinite-volume points and the black points, or the differences between  $\bar{\Pi}_r(\hat{q}^2)$  and  $\Pi_r(\hat{q}^2)$ ,  $r \in \{A_1, A_1^{44}, T_1, T_2, E\}$ , are not visible. We always omit a factor  $5e^2/9$ , equal to the sum of the squares of the charges of the up and down quarks, from Eq. (2.12), and we do the same for the lattice data.

<sup>15</sup> We recall also that only three out of the five  $\Pi_r$  and  $\bar{\Pi}_r$  are independent, because of the relations (2.9) and (2.10).

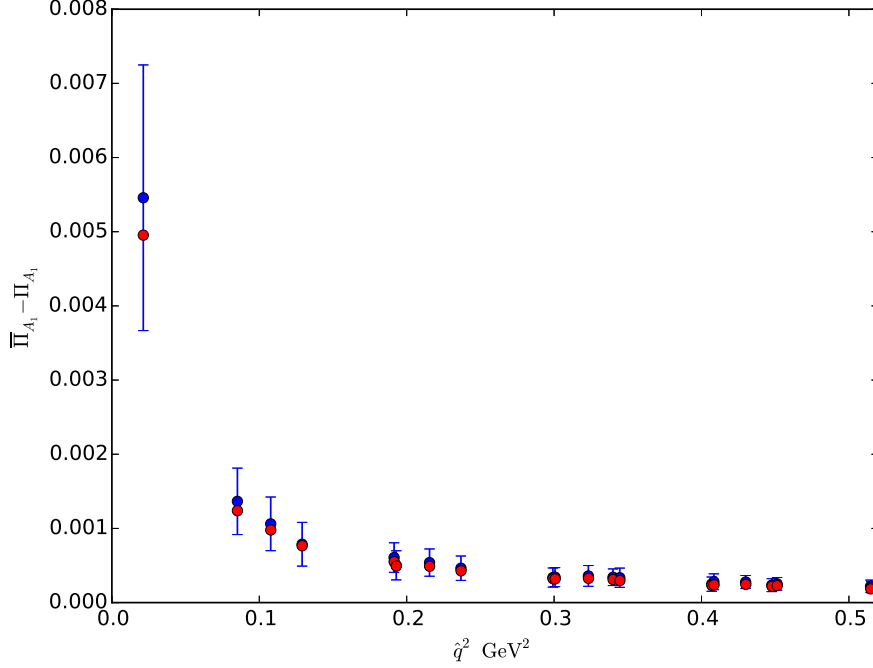


FIG. 4: Comparison of  $\bar{\Pi}_{A_1}(\hat{q}^2) - \Pi_{A_1}(\hat{q}^2)$  between MILC asqtad lattice data (blue points) and lowest-order SChPT (red points).

the continuum limit. However, the slopes are also vastly different, and this is a physical effect, already observed in Ref. [12]. The slope of the vacuum polarization at low  $q^2$  is dominated by the  $\rho$  resonance, but this resonance (and others) are absent in Eq. (2.12).<sup>16</sup>

Despite these differences, there are useful lessons to be learned from Fig. 3. The subtracted value  $\bar{\Pi}_{A_1}(\hat{q}^2)$  is an order of magnitude closer to the infinite-volume points than the unsubtracted value,  $\Pi_{A_1}(\hat{q}^2)$ . Clearly, the lesson is that one should carry out the subtraction (2.6) (at least for the  $A_1$  representation). This was already observed empirically in Ref. [22], and we see here that this observation is theoretically supported by ChPT. Furthermore, we see that  $\bar{\Pi}_{A_1}(\hat{q}^2)$  and  $\Pi_{A_1^{44}}(\hat{q}^2)$  straddle the infinite-volume result, suggesting that also in lattice QCD the true value of  $\Pi(q^2)$  lies in between these two.<sup>17</sup>

Of course, one would like to test whether these lessons from lowest-order SChPT also apply to the actual lattice data. While no lattice data are available in infinite volume, it is possible to compare finite-volume differences predicted by SChPT to such differences computed from the lattice data. In Fig. 4 we show the difference  $\bar{\Pi}_{A_1}(\hat{q}^2) - \Pi_{A_1}(\hat{q}^2)$  in the low- $\hat{q}^2$  region, both on the lattice and computed in lowest-order SChPT. This difference is a pure finite-volume effect. Clearly, SChPT does a very good job of describing the lattice data, with all red points within less than  $1\sigma$  of the blue points. This is remarkable, especially in view of the fact that lowest-order SChPT does such a poor job of describing the full lattice data for  $\Pi_{A_1}(\hat{q}^2)$ , as we noted above.

<sup>16</sup> This observation of Ref. [12] has led to the ubiquitous use of vector-meson dominance to parametrize the vacuum polarization, before model-independent methods started to be explored [4, 19–21].

<sup>17</sup>  $\Pi_r(\hat{q}^2)$  for  $r \in \{T_1, T_2, E\}$  also lies below the infinite-volume result close to  $\Pi_{A_1^{44}}(\hat{q}^2)$ , according to ChPT.

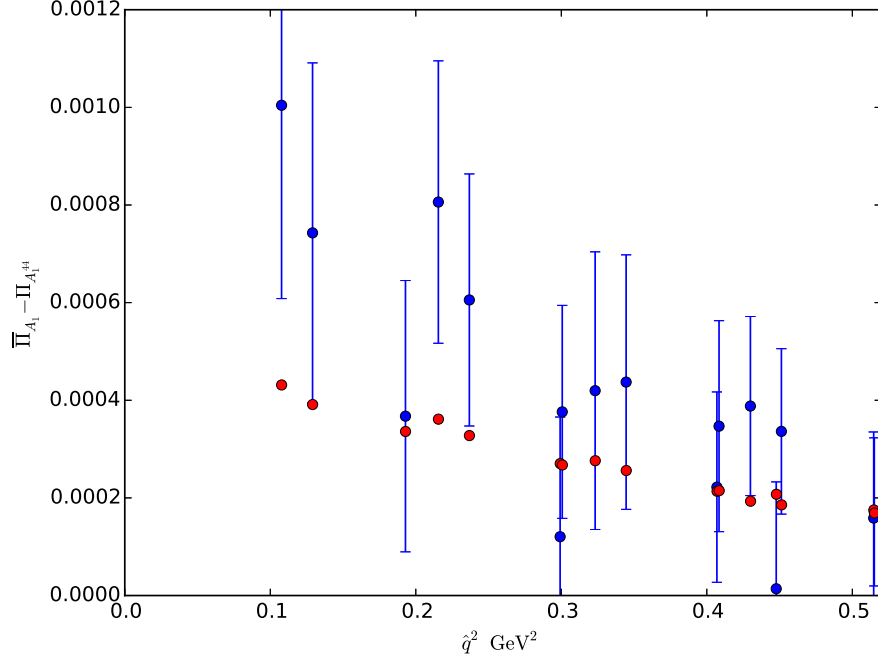


FIG. 5: Comparison of  $\bar{\Pi}_{A_1}(\hat{q}^2) - \Pi_{A_1^{44}}(\hat{q}^2)$  between MILC asqtad lattice data (blue points) and lowest-order SChPT (red points).

We may also consider differences between different representations, which also probes the size of finite-volume effects. In Fig. 5 we show the difference  $\bar{\Pi}_{A_1}(\hat{q}^2) - \Pi_{A_1^{44}}(\hat{q}^2)$ , for the lattice data, and computed in SChPT. To extract  $\Pi_{A_1^{44}}(\hat{q}^2)$  from  $\Pi_{\mu\nu}(\hat{q})$  we need at least one spatial component of the momentum to not vanish, implying that  $\hat{q}^2 \geq 4\pi^2/L^2 = 0.108 \text{ GeV}^2$  for these points. All observations made above about the difference  $\bar{\Pi}_{A_1}(\hat{q}^2) - \Pi_{A_1}(\hat{q}^2)$  apply here as well, with the difference between lattice data and ChPT now averaging about  $1\sigma$ . We note the difference of scale on the vertical axis between Figs. 4 and 5, consistent with the fact that both  $\bar{\Pi}_{A_1}(\hat{q}^2)$  and  $\Pi_{A_1^{44}}(\hat{q}^2)$  are much closer to the infinite-volume limit than  $\Pi_{A_1}(\hat{q}^2)$ . We find that the pattern is very similar for other representations.

### B. Effects on $a_\mu^{\text{HVP}}$

Finally, while it is already clear that there are significant finite-volume effects in the vacuum polarization, we consider the question of how they propagate to the anomalous magnetic moment itself. We will, in fact, compare the quantity  $a_\mu^{\text{LO,HVP}}[\hat{q}_{\text{max}}^2]$  with the choice  $\hat{q}_{\text{max}}^2 = 0.1 \text{ GeV}^2$ , in order to be certain that differences are due to finite volume, and not to lattice spacing effects.<sup>18</sup>

We fit the data for  $\bar{\Pi}_{A_1}$  and  $\Pi_{A_1^{44}}$  with a  $[0, 1]$  Padé [19], or a quadratic conformally mapped polynomial [20] (both are three-parameter fits), on a low- $q^2$  interval, looking for the number of data points in the fit that gives the highest  $p$ -value. We then compare the results.

<sup>18</sup> More than 80% of  $a_\mu^{\text{LO,HVP}}$  comes from the momentum region below  $0.1 \text{ GeV}^2$  [20].

In all the fits presented below, the number of data points in the fit turns out to be six, so all fits have three degrees of freedom, and they never explore data beyond  $\hat{q}^2 = 0.3 \text{ GeV}^2$ . As we have shown before [4, 20], neither of these two fits can be trusted to give results with a better accuracy than a few percent even in infinite volume for  $a_\mu^{\text{LO,HVP}}$ , but we will assume that other systematics are the same for both representations, so that the differences considered here measure primarily finite-volume effects. From the  $[0, 1]$  Padé fits, we find

$$\begin{aligned} a_{\mu, A_1}^{\text{LO,HVP}}[0.1 \text{ GeV}^2] &= 6.8(4) \times 10^{-8} , \\ a_{\mu, A_1^{44}}^{\text{LO,HVP}}[0.1 \text{ GeV}^2] &= 7.5(3) \times 10^{-8} . \end{aligned} \quad (3.1)$$

From the quadratic conformally mapped polynomial fits, we find

$$\begin{aligned} a_{\mu, A_1}^{\text{LO,HVP}}[0.1 \text{ GeV}^2] &= 6.8(4) \times 10^{-8} , \\ a_{\mu, A_1^{44}}^{\text{LO,HVP}}[0.1 \text{ GeV}^2] &= 7.9(4) \times 10^{-8} . \end{aligned} \quad (3.2)$$

Both types of fit give consistent results for each representation, but the two different representations differ from each other by about 10-15%. This strongly suggests that with a pion mass of 220 MeV a spatial volume with  $L = 64a = 3.8 \text{ fm}$ , or  $m_\pi L = 4.2$ , is not large enough if the aim is to compute  $a_\mu^{\text{LO,HVP}}$  with sub-percent accuracy.

#### IV. CONCLUSION

In this article, we explored finite-volume effects in the connected part of the hadronic vacuum polarization, and gave some examples of how these effects propagate to the corresponding contribution to the muon anomalous magnetic moment  $a_\mu^{\text{LO,HVP}}$ . We found that even in computations with small pion masses and  $m_\pi L > 4$ , the systematic effects due to finite volume can be of order 10%. This is consistent with the phenomenological estimate of Ref. [5].

We also found that ChPT does a good job of describing finite-volume effects already at lowest order, even though it is well known that lowest-order does not provide a good description of the vacuum polarization itself already at the low values of  $q^2$  relevant for  $a_\mu^{\text{LO,HVP}}$ . ChPT also shows that the subtracted vacuum polarization  $\bar{\Pi}_{\mu\nu}(q) = \Pi_{\mu\nu}(q) - \Pi_{\mu\nu}(0)$  is significantly closer to the infinite-volume result than  $\Pi_{\mu\nu}(q)$  itself. Projecting on irreducible representations of the cubic group, we found that in ChPT the  $A_1$  projection (after subtraction of  $\Pi_{\mu\nu}(0)$ ) and other representations (for which the subtraction makes very little difference, and is not visible in the lattice data) straddle the infinite-volume result. This leads to the question of how to quantify the systematic error due to finite volume in practice. A conservative error estimate would take half the difference between the value of  $a_\mu^{\text{LO,HVP}}$  computed from  $\bar{\Pi}_{A_1}$  and the values computed from other representations, *e.g.*  $\Pi_{A_1^{44}}$ . Because the infinite-volume result for  $\Pi$ , according to ChPT, lies between  $\bar{\Pi}_{A_1}$  and  $\Pi_{A_1^{44}}$ , a more aggressive error estimate would be obtained by taking the difference between the average of the ChPT results for  $\bar{\Pi}_{A_1}$  and  $\Pi_{A_1^{44}}$  and the infinite-volume ChPT result. However, this might be too aggressive, because the comparison of finite-volume differences between the lattice and ChPT shows that the (lowest-order) ChPT estimates the finite-volume effects we see on the lattice to about  $1\sigma$  (*cf.* Figs. 4 and 5). For lattice data with increased statistical precision, it is not clear whether lowest-order ChPT would be precise

enough, in particular for the representation  $A_1^{44}$ . It will be interesting to compare the finite-volume effects for physical pion mass and larger volume ( $L > 5$  fm). Until then it is not advisable to use ChPT to correct the lattice results.

Finally, we wish to make a comment on the “moment method,” proposed in Ref. [21]. In infinite volume,  $\Pi(0)$  can be obtained from the second moment of the current two-point function (no sum over  $i$ ),

$$\Pi(0) = -\frac{1}{2} \int dt \int d^3\vec{x} t^2 \langle J_i(\vec{x}, t) J_i(\vec{0}, 0) \rangle . \quad (4.1)$$

In a finite volume  $L^3 \times T$ , using

$$\begin{aligned} t^2 &= \sum_n a_n \cos(2\pi n t/T) , \\ a_0 &= \frac{T^2}{12} , \quad a_n = \frac{(-1)^n}{\sin^2(\pi n/T)} , \quad n \neq 0 , \end{aligned} \quad (4.2)$$

the right-hand side of Eq. (4.1) gets replaced by the expression [26]

$$\Pi(0) \rightarrow 4 \sum_{n \neq 0} (-1)^n \Pi((2\pi n/T)^2) . \quad (4.3)$$

We see that in finite volume,  $\Pi(0)$  gets replaced by a linear combination of values of  $\Pi(q^2)$  at non-zero values of  $q^2$ , not including  $q^2 = 0$ . This appears to imply that the moment method is equally susceptible to finite-volume effects.

## Acknowledgments

We thank Taku Izubuchi and Kim Maltman for useful discussions, and Luchang Jin for pointing out an error in the first version of this article. We also thank USQCD for the computing resources used to generate the vacuum polarization as well as the MILC collaboration for providing the configurations used. TB, PC and MG were supported in part by the US Department of Energy under Grant No. DE-FG02-92ER40716 and Grant No. DE-FG03-92ER40711. SP is supported by CICYTFEDER-FPA2014-55613-P, 2014-SGR-1450, the Spanish Consolider-Ingenio 2010 Program CPAN (CSD2007-00042).

## Appendix A: Vacuum polarization at one loop in ChPT

In this appendix, we derive a generalization of Eq. (2.12) for the case of twisted boundary conditions. This is a partially quenched calculation, because we will only give the valence quarks, *i.e.*, the quarks to which the external photons couple, a twist, while all sea quarks obey periodic boundary conditions. We follow the definitions and conventions of Ref. [8].<sup>19</sup> Throughout this appendix, we will use the lattice as a UV regulator, and we will express all quantities in terms of lattice units.

<sup>19</sup> See Ref. [7, 23–25] for earlier work on twisted boundary conditions for valence quarks.

We introduce six quarks,

$$q = \begin{pmatrix} u_v \\ u_t \\ d_v \\ d_t \\ u_s \\ d_s \end{pmatrix}, \quad (\text{A1})$$

where the index  $v$  labels the untwisted valence quarks, the index  $t$  labels the twisted valence quarks and the index  $s$  labels the (untwisted) sea quarks. The twisted quarks have boundary conditions

$$\begin{aligned} q_t(x) &= e^{-i\theta_\mu} q_t(x + L_\mu), \\ \bar{q}_t(x) &= \bar{q}_t(x + L_\mu) e^{i\theta_\mu}, \end{aligned} \quad (\text{A2})$$

with  $L_i = L$ ,  $i = 1, 2, 3$  and  $L_4 = T$ . Strictly speaking, one should also introduce four ghost quarks to cancel loops of the four valence quarks, but we will leave this implicit in the rest of our calculation.<sup>20</sup> Only valence quarks couple to photons, and this coupling takes the form

$$e\bar{q}\gamma_\mu(A_\mu^+Q^+ + A_\mu^-Q^-)q, \quad (\text{A3})$$

with

$$Q^+ = \begin{pmatrix} 0 & 2/3 & 0 & 0 & 0 & 0 \\ 0 & 0 & 0 & 0 & 0 & 0 \\ 0 & 0 & 0 & -1/3 & 0 & 0 \\ 0 & 0 & 0 & 0 & 0 & 0 \\ 0 & 0 & 0 & 0 & 0 & 0 \\ 0 & 0 & 0 & 0 & 0 & 0 \end{pmatrix}, \quad Q^- = \begin{pmatrix} 0 & 0 & 0 & 0 & 0 & 0 \\ 2/3 & 0 & 0 & 0 & 0 & 0 \\ 0 & 0 & 0 & 0 & 0 & 0 \\ 0 & 0 & -1/3 & 0 & 0 & 0 \\ 0 & 0 & 0 & 0 & 0 & 0 \\ 0 & 0 & 0 & 0 & 0 & 0 \end{pmatrix}. \quad (\text{A4})$$

In order to accommodate the twist, there are *two* photons, one coupling to the current  $\frac{2}{3}\bar{u}_t\gamma_\mu u_v - \frac{1}{3}\bar{d}_t\gamma_\mu d_v$ , and one coupling to the current  $\frac{2}{3}\bar{u}_v\gamma_\mu u_t - \frac{1}{3}\bar{d}_v\gamma_\mu d_t$ , corresponding to the photons going into, and out of, the vacuum polarization, which, at the valence-quark level, consists of a loop made out of a twisted up or down quark and an untwisted up or down anti-quark, thus inserting a momentum  $q_\mu + \theta_\mu/L_\mu$  with  $q$  a periodic momentum as in Eq. (2.4), and  $\theta_\mu \in [0, 2\pi)$ .

In this theory with six quarks,<sup>21</sup> the pions form a  $6 \times 6$  matrix, with flavor structure<sup>22</sup>

$$\phi \sim \begin{pmatrix} u_v\bar{u}_v & u_v\bar{u}_t & u_v\bar{d}_v & u_v\bar{d}_t & u_v\bar{u}_s & u_v\bar{d}_s \\ u_t\bar{u}_v & u_t\bar{u}_t & u_t\bar{d}_v & u_t\bar{d}_t & u_t\bar{u}_s & u_t\bar{d}_s \\ d_v\bar{u}_v & d_v\bar{u}_t & d_v\bar{d}_v & d_v\bar{d}_t & d_v\bar{u}_s & d_v\bar{d}_s \\ d_t\bar{u}_v & d_t\bar{u}_t & d_t\bar{d}_v & d_t\bar{d}_t & d_t\bar{u}_s & d_t\bar{d}_s \\ u_s\bar{u}_v & u_s\bar{u}_t & u_s\bar{d}_v & u_s\bar{d}_t & u_s\bar{u}_s & u_s\bar{d}_s \\ d_s\bar{u}_v & d_s\bar{u}_t & d_s\bar{d}_v & d_s\bar{d}_t & d_s\bar{u}_s & d_s\bar{d}_s \end{pmatrix} \sim \begin{pmatrix} & & & & \pi_{vs}^{uu} & \pi_{vs}^{ud} \\ & & & & \pi_{ts}^{uu} & \pi_{ts}^{ud} \\ & & & & \pi_{vs}^{du} & \pi_{vs}^{dd} \\ & & & & \pi_{ts}^{du} & \pi_{ts}^{dd} \\ \pi_{sv}^{uu} & \pi_{st}^{uu} & \pi_{sv}^{ud} & \pi_{st}^{ud} & & \\ \pi_{sv}^{du} & \pi_{st}^{du} & \pi_{sv}^{dd} & \pi_{st}^{dd} & & \end{pmatrix}, \quad (\text{A5})$$

<sup>20</sup> In this calculation it is not difficult to match pion loops with quark loops, so it is easy to identify contributions that should be omitted so as to suppress valence quark loops.

<sup>21</sup> And four ghost quarks.

<sup>22</sup> This equation was incorrect in the first version of this paper. This led to Eq. (A11) to be a factor 2 too small in the first version. We thank Luchang Jin for pointing this out to us.

where in the second expression we omitted all pions that do not contribute, and we used a superscript to indicate the up/down flavor structure. Note that for instance  $\pi_{vs}^{uu}$  is a charged pion, because it consists of a valence up quark with charge 2/3, and a neutral up sea anti-quark. Pure sea pions do not contribute because they are neutral.

Pions with no  $t$  subscript or with a  $tt$  subscript have periodic boundary conditions, but pions with one  $t$  subscript inherit twisted boundary conditions from Eq. (A2), for example ( $i, j = u, d$ )

$$\pi_{ts}^{ij}(x + L_\mu) = e^{i\theta_\mu} \pi_{ts}^{ij}(x) , \quad \pi_{st}^{ij}(x + L_\mu) = e^{-i\theta_\mu} \pi_{st}^{ij}(x) . \quad (\text{A6})$$

To leading order in ChPT, our calculation is equivalent to a scalar QED calculation, with lagrangian

$$\mathcal{L} = \frac{1}{2} \text{tr} (D_\mu \phi D_\mu \phi) , \quad (\text{A7})$$

with a covariant derivative accommodating the gauge invariance implied by Eq. (A3),

$$D_\mu \phi = \partial_\mu \phi + ie[A_\mu^+ Q^+ + A_\mu^- Q^-, \phi] . \quad (\text{A8})$$

It is now straightforward to carry out the desired one-loop calculation, in which the twisted vacuum polarization is defined as

$$\Pi_{\mu\nu}^{+-}(x - y) = \frac{\partial^2}{\partial A_\mu^+(x) \partial A_\nu^-(y)} \log Z \equiv e^{i\hat{\theta}(x+\mu/2-y-\nu/2)} F_{\mu\nu}^{+-}(x - y), \quad (\text{A9})$$

with  $Z$  the path integral with lagrangian (A7), and  $\hat{\theta}_\mu = \theta_\mu/L_\mu$ . Using the lattice as a regulator by replacing the covariant derivative (A8) by the nearest-neighbor covariant derivative

$$D_\mu \phi(x) = U_\mu(x) \phi(x + \mu) U_\mu^\dagger(x) - \phi(x) , \quad (\text{A10})$$

with  $U_\mu(x) = \exp[ie(A_\mu^+(x)Q^+ + A_\mu^-(x)Q^-)]$ , we find the result generalizing Eq. (2.12) for non-zero twist:

$$F_{\mu\nu}^{+-}(k) = \quad (\text{A11})$$

$$\frac{10}{9} e^2 \frac{1}{L^3 T} \sum_p \left[ \frac{4 \sin(p + (k + \hat{\theta})/2)_\mu \sin(p + (k + \hat{\theta})/2)_\nu}{(2 \sum_\kappa (1 - \cos p_\kappa) + m_\pi^2) (2 \sum_\kappa (1 - \cos(p + k + \hat{\theta})_\kappa) + m_\pi^2)} \right. \\ \left. - \delta_{\mu\nu} \left( \frac{\cos p_\mu}{(2 \sum_\kappa (1 - \cos p_\kappa) + m_\pi^2)} + \frac{\cos(p + \hat{\theta})_\mu}{(2 \sum_\kappa (1 - \cos(p + \hat{\theta})_\kappa) + m_\pi^2)} \right) \right] .$$

In the infinite-volume limit, this result agrees with that of Ref. [27].

It is easy to verify that for  $L, T \rightarrow \infty$ ,  $F_{\mu\nu}^{+-}(0) = 0$ . The sum in Eq. (A11) becomes an integral,  $\hat{\theta} \rightarrow 0$ , and we can partially integrate the first term to cancel against the second. But, in a finite volume, these simplifications do not apply. For zero twist,  $\theta_\mu = 0$ , it is straightforward to estimate  $F_{\mu\nu}^{+-}(0) = \Pi_{\mu\nu}(0)$  analytically. Only the diagonal terms do not vanish, and  $\Pi_{ii}(0) \gg \Pi_{44}(0)$  if  $T \gg L$ . We will therefore choose  $\mu = \nu = 1$ . Using

$$\sum_{n=-\infty}^{\infty} \delta(x - n) = \sum_{n=-\infty}^{\infty} e^{2\pi i n x} , \quad (\text{A12})$$

and denoting the expression inside square brackets in Eq. (A11) for  $\theta_\mu = 0$  and  $q = 0$  as  $f_{\mu\nu}(p)$ , Eq. (A11) can be rewritten as (dropping the factor  $10e^2/9$ )

$$\frac{1}{L^3 T} \sum_p f_{11}(p) = \frac{1}{(2\pi)^4} \sum_n \int d^4 p f_{11}(p) e^{inLp} , \quad (\text{A13})$$

where  $nLp = \sum_\mu n_\mu L_\mu p_\mu$ . The term with  $n = 0$  is the infinite volume result, and the terms with  $n \in \{(\pm 1, 0, 0, 0), (0, \pm 1, 0, 0), (0, 0, \pm 1, 0)\}$  constitute the dominant finite-volume correction. Focussing on these terms, we can take the continuum limit, yielding the intermediate result

$$\frac{1}{(2\pi)^4} \int d^4 p \left( \frac{4p_1^2}{(p^2 + m_\pi^2)^2} - \frac{2}{p^2 + m_\pi^2} \right) (2e^{iLp_1} + 4e^{iLp_2}) . \quad (\text{A14})$$

Carrying out the integral over  $p_1$  we find that the integral with the factor  $e^{iLp_2}$  vanishes (by partial integration on  $p_1$  of the first term), and this expression reduces to

$$-2L \frac{1}{(2\pi)^3} \int d^3 p e^{-L\sqrt{m_\pi^2 + \vec{p}^2}} = -\frac{m_\pi^2}{\pi^2} K_2(m_\pi L) , \quad (\text{A15})$$

where  $K_2(z)$  is a modified Bessel function of the second kind. Using its asymptotic expansion for large argument, we find that (*cf.* Eq. (2.5))

$$\Pi_s(0) = \Pi_{11}(0) \sim -\frac{10e^2}{9} \frac{m_\pi^2}{\pi^2} \sqrt{\frac{\pi}{2m_\pi L}} e^{-m_\pi L} \left( 1 + O\left(\frac{1}{m_\pi L}\right) \right) . \quad (\text{A16})$$

- 
- [1] T. Blum, Phys. Rev. Lett. **91**, 052001 (2003) [hep-lat/0212018].
  - [2] B. E. Lautrup, A. Peterman and E. de Rafael, Nuovo Cim. A **1**, 238 (1971).
  - [3] T. Blum, T. Izubuchi and E. Shintani, Phys. Rev. D **88**, no. 9, 094503 (2013) [arXiv:1208.4349 [hep-lat]].
  - [4] M. Golterman, K. Maltman and S. Peris, Phys. Rev. D **88**, no. 11, 114508 (2013) [arXiv:1309.2153 [hep-lat]].
  - [5] A. Francis, B. Jaeger, H. B. Meyer and H. Wittig, Phys. Rev. D **88**, 054502 (2013) [arXiv:1306.2532 [hep-lat]].
  - [6] C. Aubin, T. Blum, P. Chau, M. Golterman, S. Peris and C. Tu, arXiv:1510.05319 [hep-lat].
  - [7] M. Della Morte, B. Jäger, A. Jüttner and H. Wittig, JHEP **1203**, 055 (2012) [arXiv:1112.2894 [hep-lat]].
  - [8] C. Aubin, T. Blum, M. Golterman and S. Peris, Phys. Rev. **D88**, 074505 (2013) [arXiv:1307.4701 [hep-lat]].
  - [9] E. Shintani, S. Aoki, H. Fukaya, S. Hashimoto, T. Kaneko, T. Onogi and N. Yamada, Phys. Rev. D **82**, 074505 (2010) [arXiv:1002.0371 [hep-lat]].
  - [10] D. Bernecker and H. B. Meyer, Eur. Phys. J. A **47**, 148 (2011) [arXiv:1107.4388 [hep-lat]].
  - [11] M. Golterman, arXiv:0912.4042 [hep-lat].
  - [12] C. Aubin and T. Blum, Phys. Rev. D **75**, 114502 (2007) [hep-lat/0608011].
  - [13] D. Boito, M. Golterman, M. Jamin, K. Maltman and S. Peris, Phys. Rev. D **87**, no. 9, 094008 (2013) [arXiv:1212.4471 [hep-ph]].



- [14] W. J. Lee and S. R. Sharpe, Phys. Rev. D **60**, 114503 (1999) [hep-lat/9905023].
- [15] C. Aubin and C. Bernard, Phys. Rev. D **68**, 034014 (2003) [hep-lat/0304014].
- [16] M. Golterman, PoS CONFINEMENT **8**, 014 (2008) [arXiv:0812.3110 [hep-ph]].
- [17] MILC collaboration, <http://physics.indiana.edu/~sg/milc.html> .
- [18] A. Bazavov *et al.* [MILC Collaboration], arXiv:1503.02769 [hep-lat].
- [19] C. Aubin, T. Blum, M. Golterman and S. Peris, Phys. Rev. D **86**, 054509 (2012) [arXiv:1205.3695 [hep-lat]].
- [20] M. Golterman, K. Maltman and S. Peris, Phys. Rev. D **90**, no. 7, 074508 (2014) [arXiv:1405.2389 [hep-lat]].
- [21] B. Chakraborty *et al.* [HPQCD Collaboration], Phys. Rev. D **89**, no. 11, 114501 (2014) [arXiv:1403.1778 [hep-lat]].
- [22] R. Malak *et al.* [Budapest-Marseille-Wuppertal Collaboration], PoS LATTICE **2014**, 161 (2015) [arXiv:1502.02172 [hep-lat]].
- [23] P. F. Bedaque, Phys. Lett. B **593**, 82 (2004) [nucl-th/0402051].
- [24] G. M. de Divitiis, R. Petronzio and N. Tantalo, Phys. Lett. B **595**, 408 (2004) [hep-lat/0405002].
- [25] C. T. Sachrajda and G. Villadoro, Phys. Lett. B **609**, 73 (2005) [hep-lat/0411033].
- [26] T. Blum and T. Izubuchi, private notes (2015).
- [27] M. Della Morte and A. Jüttner, JHEP **1011**, 154 (2010) [arXiv:1009.3783 [hep-lat]].